

Pair production in inhomogeneous fields

Holger Gies and Klaus Klingmüller

*Institut für theoretische Physik, Universität Heidelberg
Philosophenweg 16, D-69120 Heidelberg, Germany*

October 2, 2018

Abstract

We employ the recently developed worldline numerics, which combines string-inspired field theory methods with Monte Carlo techniques, to develop an algorithm for the computation of pair-production rates in scalar QED for inhomogeneous background fields. We test the algorithm with the classic Sauter potential, for which we compute the local production rate for the first time. Furthermore, we study the production rate for a superposition of a constant E field and a spatially oscillating field for various oscillation frequencies. Our results reveal that the approximation by a *local* derivative expansion already fails for frequencies small compared to the electron mass scale, whereas for strongly oscillating fields a derivative expansion for the *averaged* field represents an acceptable approximation. The worldline picture makes the nonlocal nature of pair production transparent and facilitates a profound understanding of this important quantum phenomenon.

1 Introduction

Pair production was first proposed for electron-positron pairs in strong, temporally and spatially constant electric fields [1, 2, 3]. Today it is often referred to as the Schwinger [4] mechanism. As a nonperturbative mechanism, pair production is of great theoretical interest. From a phenomenological point of view, it corresponds to probing the theory in the domain of strong fields. Consequently, we encounter pair production in many topics of contemporary physics, for instance, black hole evaporation [5] and e^+e^- creation in the vicinity of charged black holes [6, 7] as well as particle production in hadronic collisions [8] and in the early universe [9, 10]. Since QED pair production in strong fields represents the conceptually simplest case, it can serve as a theoretical laboratory for all these cases.

A sizeable rate for spontaneous pair production requires extraordinary strong electric fields, comparable in size to the so-called critical field strength, which corresponds to the electron-mass scale, $E_{\text{cr}} = m^2/e \approx 1.3 \cdot 10^{18} \frac{\text{V}}{\text{m}}$. For a long time, it seemed inconceivable to produce macroscopic electric fields of the required strength in the laboratory, but today, with the development of strong lasers, there are several promising experiments in progress [11, 12, 13]; for a discussion of experimental requirements, see [14].

Many different theoretical methods, such as the proper-time method [4, 15], WKB techniques [16, 17, 18, 19], the Schrödinger-Functional approach [20], functional techniques [21, 22], kinetic equations [23, 24, 25, 26], various instanton techniques [27, 28, 29, 30], Borel summation [31, 32], and propagator constructions [33, 34], have been developed to study pair production in external fields. Also, finite-temperature contributions have been determined which first occur at the two-loop level [35, 36]. Of particular conceptual interest is the production rate in terms of the effective action for a given background, which is also used in this work. Owing to an intimate relation between the effective action and the vacuum-persistence amplitude, it is the imaginary part of the effective action that encodes information about pair production which, in this context, is

interpreted as spontaneous vacuum decay. This approach yields the instantaneous production rate, neglecting back-reactions and memory effects. However, this rate can serve as a source term for kinetic equations, which can then take back-reactions and memory effects into account [23, 24, 25, 26].

Even though the existing methods follow a well defined and technically stringent concept, their application often faces serious technical and conceptual difficulties. Up to now, no reliable and universal method—be it analytic or numeric—is available for the calculation of pair-production rates in inhomogeneous electric fields. In standard approaches, functional traces have to be evaluated with the knowledge of the spectrum of the corresponding differential operator, which is only available for special cases. Moreover, controlling the divergencies that possibly occur upon summing up the eigenvalues is a delicate task.

In the present work, we solve these problems by using the recently developed numerical worldline techniques [37, 38, 39, 40, 41] which are based on the string-inspired worldline formalism [42, 43, 44, 45, 46, 47, 48, 49, 50]. The important advantage compared to other approaches lies in the fact that worldline numerics can be formulated independently of any symmetry of the background. The identification of and the summation over the spectrum of quantum fluctuations are done in one single and finite step. For simplicity, we confine ourselves to scalar QED; generalization to spinor QED is, in principle, straightforward and will be discussed below.

Beyond the computational advantages of worldline techniques, the worldline picture also helps to understand conceptual aspects in more depth. In particular, the nature and the role of nonlocalities become highly transparent from the worldline viewpoint, since the worldlines themselves represent extended virtual trajectories of the fluctuating particles in coordinate space. In the present context, we are aiming at the quantum effective action which, of course, receives nonlocal contributions in general. However, many standard approximation methods suppress (or shade) nonlocalities by construction, as, e.g., the derivative expansion. Hence, pair production as described by the Schwinger formula is often recognized as a nonperturbative phenomenon, but not so much as a nonlocal phenomenon. Nevertheless, the latter property is crucial, as the following heuristic argument elucidates: in order for a virtual pair to become real, i.e., on-shell, the pair must gain at least the amount of $2m$ of energy; this is only possible by propagating in opposite directions in the electric field. This delocalization of the pair wave function is mandatory for gaining sufficient energy.

In constant electric fields, this delocalization remains invisible in the final result. By contrast, in inhomogeneous fields the spacetime dependence of the delocalized wave function matters a great deal and can even dominate the resulting effect, as our results demonstrate. In the worldline picture, the nonlocal effects already become transparent on the level of the formalism, since the extended worldlines exactly describe the delocalization of a virtual pair.

At this point, we would like to stress the difference of the present work to earlier applications of worldline numerics. Whereas the algorithms developed so far in [37, 38, 39, 40, 41] have proven their capabilities for computing the real part of the effective action (and action densities), the computation of the imaginary part is by no means a straightforward generalization. The reason for this lies in the truly Minkowskian nature of the problem of pair production: vacuum decay only occurs for real, i.e., Minkowskian, electric fields. This contrasts with the indispensable necessity of a Euclidean formulation for solving the worldline integrals by a statistical Monte Carlo algorithm. In practice, this results in an overlap problem: the finite Euclidean worldline ensemble can have little overlap with those worldlines that contribute dominantly to Minkowski-valued observables. We solve this fundamental problem by resorting to a technique developed in [51] in the different context of nonperturbative Euclidean worldline numerics: we fit a suitable cumulative density function (CDF) of the Euclidean ensemble to a physically motivated ansatz that can be continued analytically to Minkowski space. We should emphasize that this continuation represents an extrapolation of certain ensemble properties to Minkowski space which is an a priori uncontrolled procedure resulting in systematic errors. We check this extrapolation carefully against various analytically known results and find negligibly small systematic errors compared to the statistical Monte Carlo errors. Hence, we regard the overlap problem as solved for the present problem. This solution is obtained at the expense of numerical cost; moreover, the algorithm

can, in principle, not be made arbitrarily precise, in contrast to former applications of worldline numerics. Nevertheless, for the problem of pair production and as far as the experimentally required accuracy is concerned, we believe that our algorithm is sufficiently powerful.

2 Worldline formalism for pair production

The vacuum-persistence amplitude can be related to the effective action Γ_M in Minkowski space,

$$\langle \Omega | e^{-iHT} | \Omega \rangle = e^{i\Gamma_M}.$$

The corresponding probability for the vacuum to decay spontaneously is

$$P = 1 - e^{-2\text{Im}\Gamma_M}.$$

In the case of QED with electric background fields, vacuum decay occurs in the form of spontaneous pair production, the production rate per unit time and volume of which is directly proportional to the imaginary part of the effective action density (effective Lagrangian).

In scalar QED, the one-loop contribution to the Euclidean effective action Γ_E reads

$$\Gamma_E^1[A] = \ln \det \left(-(\partial + ieA)^2 + m^2 \right), \quad (1)$$

where Γ_M and Γ_E differ by a minus sign, $\Gamma_M = -\Gamma_E$. In the worldline approach, the logarithm of the determinant in D -dimensional spacetime is represented by a path integral [50],

$$\Gamma_E^1[A] = -\frac{1}{(4\pi)^{D/2}} \int_0^\infty \frac{dT}{T^{1+D/2}} e^{-m^2 T} \int_{x(0)=x(T)} \mathcal{D}x(\tau) e^{-\int_0^T d\tau \left(\frac{\dot{x}^2}{4} + ie\dot{x}A(x) \right)}, \quad (2)$$

where the integration parameter T is called the proptime. The path integral runs over all closed worldlines, parameterized by the proptime. The worldlines can be viewed as the trajectories of the virtual fluctuations in coordinate space. The path integral is normalized to give 1 in the limit of zero gauge potential. We split the path integral into an integral over all paths with a common center of mass x_0 and an ordinary integral over all x_0 , $x(\tau) \rightarrow x_0 + x(\tau)$, where $\int_0^T d\tau x(\tau) = 0$. Introducing the *Wilson loop*,

$$W_{x_0}[x(\tau)] := e^{-ie \int_0^T d\tau \dot{x}A(x_0+x(\tau))}, \quad (3)$$

and its *expectation value*,

$$\langle W_{x_0} \rangle := \int_{\substack{x(0)=x(T) \\ \text{CM}}} \mathcal{D}x(\tau) W_{x_0}[x(\tau)] e^{-\int_0^T d\tau \frac{\dot{x}^2}{4}}, \quad (4)$$

we can write:

$$\Gamma_E^1[A] = -\frac{1}{(4\pi)^{D/2}} \int d^D x_0 \int_0^\infty \frac{dT}{T^{1+D/2}} e^{-m^2 T} \langle W_{x_0} \rangle + \text{c.t.} \quad (5)$$

Here we have added counterterms (c.t.) which have to be fixed by renormalization of physical parameters. If the electric field is nonzero, $\Gamma^1[A]$ obtains an imaginary part, arising from poles of the Wilson-loop expectation value $\langle W_{x_0} \rangle$ on the real T axis. Surrounding the poles by halfcircles in the upper half plane in agreement with causality leads to

$$\text{Im}\Gamma_E^1[A] = -\frac{1}{(4\pi)^{D/2}} \int d^D x_0 \text{Im} \sum_{T_{\text{pol}}} \frac{1}{T_{\text{pol}}^{1+D/2}} e^{-m^2 T_{\text{pol}}} (-\pi i) \text{Res}(\langle W_{x_0} \rangle, T_{\text{pol}}), \quad (6)$$

where the sum goes over all poles with positions T_{pol} . The exponential factor with Gaussian velocity weight in the path integral in Eq. (4) suppresses the contribution of long paths. Therefore, the

integral is dominated by paths that tightly wiggle around the common center of mass. This gives rise to the picture of a *loop cloud* sitting at x_0 and scanning the background field in the neighborhood of x_0 . Hence, the nonlocal nature of the phenomenon is already apparent in the formalism.

Let us mention in passing that the path integral for a constant E background is Gaussian, can thus be done exactly, and results in $\langle W_{x_0} \rangle = eET / \sin(eET)$; see below. Summing over the pole positions of the inverse sine results in the famous Schwinger formula (for scalar QED in this case),

$$\text{Im}\Gamma_{\text{M}}^1[E = \text{const.}] = -\frac{V}{16\pi^3} (eE)^2 \sum_{n=1}^{\infty} \frac{(-1)^n}{n^2} e^{-\frac{m^2}{eE} \pi n}, \quad (7)$$

displaying the nonperturbative dependence on eE [4]; here, V denotes the space-time volume. Each term in the sum corresponds to production of n coherent pairs.

3 Worldline numerics

3.1 Worldline discretization

The worldline numerical algorithm for the present problem partly resembles closely those developed in detail in [37, 38, 39, 40, 41], the essential steps of which we will recall in the following for completeness. As a first step, we introduce the *unit loop* $y(t)$,

$$y(t) := \frac{1}{\sqrt{T}} x(Tt). \quad (8)$$

The Wilson-loop expectation value then reads

$$\langle W_{x_0} \rangle := \int_{y(0)=y(1)}^{\text{CM}} \mathcal{D}y(t) W_{x_0} e^{-\int_0^1 dt \frac{\dot{y}^2}{4}}. \quad (9)$$

The exponential velocity distribution is now independent of T , whereas the Wilson loop yields

$$W_{x_0} = e^{-ie \int_0^1 dt \sqrt{T} \dot{y} A(\sqrt{T} y + x_0)}. \quad (10)$$

For a finite ensemble of paths that are distributed according to the weight factor $\exp(-\int_0^1 d\tau \frac{\dot{y}^2}{4})$, the Wilson-loop expectation value is equal to the arithmetic ensemble average of W_{x_0} . Since the weight factor for unit loops is independent of T and x_0 , such a loop ensemble has to be generated only once for computing $\langle W_{x_0} \rangle$ for different T and x_0 .

For the numerics, we discretize the proptime such that each loop $y(t)$ is represented by a finite number of N points per loop (ppl) y_k at $t = k/N$, with $k = 1, \dots, N$.¹ We use the *vloop* algorithm [40] to create an ensemble of n_L discrete and closed unit loops $\{y_k\}$ with the distribution functional

$$P[\{y_k\}] = \delta(y_1 + \dots + y_N) \exp\left(-\frac{N}{4} \sum_{k=1}^N (y_k - y_{k-1})^2\right), \quad (11)$$

with the condition $y_0 \equiv y_N$ for closed loops. Eq. (11) represents the discrete form of the weight factor $\exp(-\int_0^1 d\tau \frac{\dot{y}^2}{4})$, with the delta function reflecting the center-of-mass condition.

For a gauge-invariant discretization of the Wilson loop, the gauge field, in principle, should be treated as a link variable, i.e., $dt \dot{y}(t) A(y(t)) \rightarrow (y_k - y_{k-1}) A((y_k + y_{k-1})/2)$, with the gauge field evaluated at the center of the links. However, the link centers do not carry the same information about the distribution of the worldlines in spacetime as the sites y_k do: for instance, the link centers have a smaller average distance to the center of mass x_0 than the sites do. The use of the

¹The worldline points y_k live in continuous space-time, $y_k \in \mathbb{R}^D$. For an alternative lattice formulation, see [52, 53].

link centers actually corresponds to effectively shrinking the loop cloud. Of course, this difference becomes irrelevant in the proper-time continuum limit $N \rightarrow \infty$. However, for small N , this effect leads to sizeable systematic deviations from the continuum limit. We avoid this systematic by evaluating the gauge field at the sites instead,

$$\int_0^1 dt \dot{y} A(\sqrt{T}y + x_0) \rightarrow \sum_{k=1}^N (y_{k+1} - y_k) A(\sqrt{T}y_k + x_0). \quad (12)$$

It turns out that possible violations of gauge invariance for smooth gauges such as the Lorenz gauge remain much smaller than other systematic and statistical errors for the background fields studied in this work.²

For the effective action and the pair-production rate, the T integration in Eq. (5) has to be performed. For the simple case of a constant field, this can be done elegantly by a fast-Fourier transform (FFT) after the T integration has been rotated onto the imaginary axis. Thereby, the pair production is obtained for a whole spectrum of masses and field strengths, respectively, all at once. This procedure and its limitations will be discussed in the Appendix. However, for more general field configurations, an overlap problem arises: when performing the T integration, one faces situations in which the path integral is dominated by very elongated loops, despite the exponential suppression by the weight factor. Physically, those virtual pairs that delocalize strongly gain more energy and have a larger probability of becoming real. In this case, the finite loop ensemble with only a few elongated worldlines is no longer representative for the over-countably many paths of the path integral. To solve this problem, we have developed the routine presented in the following. Its cornerstone is a probability distribution analysis of particular worldline-ensemble properties along the lines suggested in [51].

3.2 CDF fit for pair production

In order to motivate our algorithm, let us first consider the case of a constant homogeneous electric field E in Minkowski space.³ This is related to the Euclidean gauge potential by $A|_E = (0, 0, 0, -iEx_1)^\top$. The corresponding Wilson loop can be written as

$$W(I) = e^{-TeEI}, \quad \text{where } I := \int_0^1 dt \dot{y}_4 y_1. \quad (13)$$

The scalar quantity I contains all relevant information about the unit loop for the present case. The probability density function (PDF) of I for our loop ensembles is defined by

$$P(I) = \int_{\substack{y(0)=y(1) \\ \text{CM}}} \mathcal{D}y \delta\left(I - \int_0^1 dt \dot{y}_4 y_1\right) e^{-\int_0^1 dt \frac{\dot{y}^2}{4}}. \quad (14)$$

With the aid of a Fourier representation of the δ function, the path integral becomes Gaussian and yields

$$P(I) = \frac{\pi}{4} \cosh^{-2}\left(\frac{\pi}{2}I\right) \quad (15)$$

for constant fields. In terms of the PDF, the Wilson-loop expectation value can be written as

$$\langle W \rangle = \int_{-\infty}^{\infty} dI P(I) W(I), \quad (16)$$

resulting in $\langle W \rangle = TeE/\sin(TeE)$ in agreement with the Schwinger pair-production rate for constant fields, cf. Eq (7).

²In the general case, we, of course, recommend the gauge-invariant link variable discretization. In order to reduce the systematic error mentioned above, order $1/N$ improvements of the action may be useful.

³ E denotes the *Minkowskian*, i.e., *physical*, field strength.

For inhomogeneous field configurations, $\langle W_{x_0} \rangle$ can be computed in a similar way. Generalizing the definition of I ,

$$I_{x_0} := \frac{i \int_0^1 dt \dot{y} A(\sqrt{T}y + x_0)}{\sqrt{T}E_0}, \quad (17)$$

the PDF becomes space-time and proper-time dependent,

$$P_{x_0}(I) = \int_{y^{(0)}=y^{(1)}_{\text{CM}}} \mathcal{D}y \delta(I - I_{x_0}) e^{-\int_0^1 dt \frac{\dot{y}^2}{4}}. \quad (18)$$

But for each space-time point, the Wilson-loop average can still be computed analogously to Eq. (16), with $W(I) = e^{-TeE_0 I}$ similar to Eq. (13). The reference field strength E_0 is a priori arbitrary and has been introduced to obtain a dimensionless quantity. In most cases, we may use the local field strength $E_0 := |E(x_0)|$, or some averaged value. For the constant E field, our generalized definition of I_{x_0} conforms to the previous one. The PDF of I_{x_0} is generally not known analytically but will be computed numerically from a finite loop ensemble. Nevertheless, analytical knowledge about $P_{x_0}(I)$ is required, owing to the following reasons:

- The use of a Monte Carlo algorithm does not only demand the worldline spacetime metric to be Euclidean, but also requires the contour of the proptime integral to run along the real T axis. However, as is already obvious for the constant-field case, the integral in Eq. (16) is well defined only for $|TeE| < \pi$. At $|TeE| = \pi$, the first pole T_{pol} of $\langle W_{x_0} \rangle$ is hit. For larger values of $|eET|$, the I integral has to be replaced by its analytic continuation, which can only be constructed if $P_{x_0}(I)$ is known analytically.
- By using *finite* loop ensembles, we already face an overlap problem for small T values: the majority of loops have a small I value, whereas those few loops with large I dominate the I integral in Eq. (16); see the Appendix. A controlled extrapolation of the PDF to large I values from reasonably big worldline ensembles can thus reduce the numerical cost considerably. This can be achieved by fitting the numerical PDF data to an analytical ansatz.

The last point is, of course, related to the nonlocal features of pair production. The quantity I on the one hand is connected to the electrostatic energy gain of a virtual pair that propagates in a background field, and on the other hand roughly measures the space-time extent of a worldline. The dominance of large I values in the final result arises from strongly delocalized virtual pairs.

To obtain an analytical estimate for the PDF, we generalize the result for the constant field, Eq. (15), by the following ansatz governed by two parameters α and ν :

$$P_{x_0}(I) = N \cosh^{-2\nu} \left(\frac{\pi}{2} \alpha I \right). \quad (19)$$

The parameters control the two main features of the distribution: width and sheerness. Both parameters depend on the spacetime point x_0 and on the proptime parameter T . The normalization constant N is a function of α and ν fixed by $\int dI P_{x_0}(I) = 1$. Numerically more convenient is the corresponding cumulative density function (CDF) of $|I|$,

$$D_{x_0}(|I|) = \int_{-|I|}^{|I|} d\hat{I} P(\hat{I}).$$

For given values T and x_0 , we determine α and ν by a fit of the numerical data to this CDF. Inserting the resulting parameters into Eq. (19) yields the desired analytical expression for $P_{x_0}(I)$. Performing the I integral in Eq. (16) gives $\langle W_{x_0} \rangle$ as function of α and ν ,

$$\langle W_{x_0} \rangle = N \frac{4^\nu}{\pi \alpha} \frac{\Gamma(\nu + \frac{TeE_0}{\pi \alpha}) \Gamma(\nu - \frac{TeE_0}{\pi \alpha})}{\Gamma(2\nu)}.$$

This result also represents the desired analytical continuation to arbitrary values of T or $|eE_0T|$, and solves the problem of Wick rotating the result of the Euclidean path integral back to Minkowski space. We observe that the second Gamma function in the numerator is responsible for the pole structure of $\langle W_{x_0} \rangle$ on the positive real axis. Poles occur if

$$\nu - \frac{TeE_0}{\pi\alpha} = -l, \quad \text{with } l = 0, 1, 2, \dots \quad (20)$$

Since α and ν depend on T , Eq. (20) determines the pole positions T_{pol} only implicitly; in practice, we solve for T_{pol} iteratively. At the pole location, the corresponding residue is

$$\text{Res}(\langle W_{x_0} \rangle, T_{\text{pol}}) = N \frac{4^\nu}{\pi\alpha} \frac{\Gamma(2\nu + l)}{\Gamma(2\nu)} \frac{(-1)^l}{l! \frac{d}{dT} \left(\nu - \frac{TeE_0}{\pi\alpha} \right)} \Big|_{T_{\text{pol}}},$$

which we plug into Eq. (6) to obtain the pair-production rate. For a reliable control of the statistical error, we perform a jackknife analysis for all secondary quantities. For the systematic error due to the proper-time discretization, we increase the number of N ppl to approach the continuum limit at least within the statistical errors.

Obviously, the reliability of our results depends crucially on the ansatz (19) for the PDF. Apart from our consistency arguments referring to the shape of the PDF and the resulting pole structure, final support can only be given by nontrivial tests described below. In summary, the sufficiency of the ansatz is confirmed by the following arguments:

- The free parameters control the two most essential features of the distribution, the width and the sheerness, which encode, in particular, the important contributions from the strongly delocalized virtual pairs.
- The exact functional form for the constant-field limit is supported by the ansatz. Even without further checks, we could thus expect satisfactory results at least for slowly varying fields.
- As a nontrivial analytical confirmation, we stress that the ansatz leads to a reasonable pole structure of $\langle W \rangle$ that can encode information about coherent n pair production.
- The ansatz provides highly convincing results for the Sauter potential including the constant field limit as special case, as presented in the next section. Any systematic deviations from the exact result are negligibly small compared to the statistical error.

4 Sauter potential

The Sauter potential defines an electric field with solitonic profile in one spatial direction which is constant in all other directions including time. The direction of the field vector is constant and coincides with the solitonic-profile direction. An analytical expression of the corresponding total pair-production rate has been found by Nikishov [54]. In Minkowski space, the Sauter potential reads

$$A^0|_{\text{M}} = -a \tanh(kx^1), \quad A^i|_{\text{M}} = 0, \quad E^1|_{\text{M}} = \frac{ak}{\cosh^2(kx^1)}.$$

The parameter k defines the inverse width of the electric field, whereas a governs its maximum, $E_{\text{max}} \equiv ak$. The constant-field limit is recovered for $k \rightarrow 0$ for fixed ak .

As an example, Fig. 1 shows the x_1 dependence of the local pair-production rate $\sim \text{Im}\mathcal{L}_{\text{eff}}$ for $k = 0.4m$ and $E_{\text{max}} \equiv ak = (m^2/e)$ computed by our algorithm. It is compared to the approximated effective Lagrangian obtained by a derivative expansion to lowest order, i.e., by assuming the field to be locally constant (Schwinger formula). We observe that the local rate predicted by the algorithm is spatially smeared compared to the Schwinger formula.

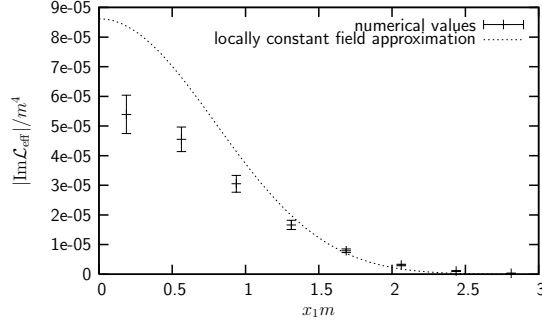


Figure 1: Spatial distribution of the effective Lagrangian's imaginary part for a Sauter potential. The numerical result is compared to the locally constant-field approximation that overestimates the true result by up to $\sim 50\%$. Parameters of the Sauter potential: $k = 0.4m$, $E_{\max} = (m^2/e)$. Parameters of the loop cloud: $n_L = 100000$, $N = 1000$ ppl.

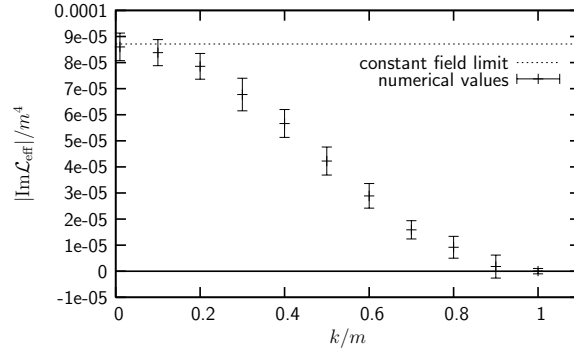


Figure 2: The imaginary part of the effective Lagrangian in the center of a Sauter potential with maximal field strength m^2/e versus the inverse width parameter k . The dashed line marks the analytically obtained contribution of the first pole to $|\text{Im}\mathcal{L}_{\text{eff}}|$ for the constant-field limit (higher poles give a 1% correction). $n_L = 100000$, $N = 1000$ ppl.

The pair-production density in the center $x^1 = 0$ of the Sauter potential with maximal field strength $E_{\max} = (m^2/e)$ is shown in Fig. 2 versus the width parameter k ; units are set by the electron mass scale. For large width $k \rightarrow 0$, the constant-limit is approached, and our CDF fit algorithm correctly reproduces the Schwinger formula. The more interesting limit occurs for $k = m$ where the production rate vanishes. Even though the electric field is still nonzero, the width of the Sauter potential is equal to the Compton wavelength. Therefore, even if a virtual pair delocalizes completely along the direction of field lines with the e^- going to $x^1 \rightarrow \infty$ and the e^+ going to $-\infty$, the pair cannot acquire enough energy to become real. This important physical example is missed completely by the locally constant-field approximation, emphasizing the role of nonlocalities.

Moreover, the limiting case of $k \rightarrow m$ is an extreme and crucial test for our algorithm based on the PDF ansatz (19): in the vicinity of this limit, there is literally not a single worldline in our finite ensemble that exhibits the strong delocalization required for giving rise to a *direct* contribution to the final result (the number of sufficiently elongated worldlines is exponentially suppressed). Nevertheless, the overall distribution of I values allows for a controlled extrapolation via the CDF fit, leading to a numerical estimate even for the directly inaccessible regime. As a measure for the resulting error, we mention that our result for the case $k = m$ is not exactly zero, but $|\text{Im}\mathcal{L}_{\text{eff}}|/m^4 = 5.73 \cdot 10^{-8} \pm 1.03 \cdot 10^{-6}$. We conclude that possible systematic errors induced by our CDF fit algorithm are negligibly small compared to the statistical error.

Finally, Fig. 3 shows the integrated total pair-production rate $\text{Im}\Gamma$ compared to the Nikishov

result. The agreement is satisfactory and the vanishing pair production for $ea = m$ is reproduced within the error bars.

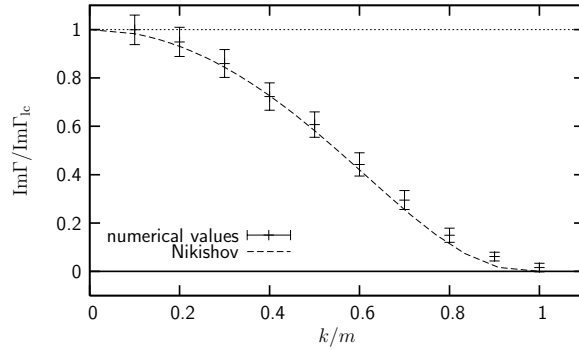


Figure 3: The imaginary part of the effective action for a Sauter potential as fraction of the locally constant-field approximation $\text{Im}\Gamma_{lc}$ versus the width parameter k in units of m : comparison of the numerical result with Nikishov's analytic expression. $n_L = 100000$, $N = 1000$ ppl.

5 Sine-modulated potential

In this section, we study the superposition of a spatially varying sine potential with a constant field. This configuration is of general interest, as it is representative for a class of field configurations which are superpositions of a slowly varying field—in our example the constant field—and higher-oscillation modes. A very important aspect is the dependence of the pair-production rate on the spatial oscillation frequency of the small-scale field structures. We consider this example as a paradigm for the role of nonlocal phenomena in pair production.

In Minkowski space, the potential is given by

$$A^0|_M = -a \sin(kx^1) - E_0 x^1, \quad A^i|_M = 0.$$

It corresponds to an E field in x^1 direction with field strength

$$E^1|_M = E_0 + ak \cos(kx^1),$$

which has extremal field strength of $E_{\max, \min} = E_0 \pm ak$. As an example, we study a field with $E_0 = 0.2(m^2/e)$ and $E_{\max} = 0.3(m^2/e)$.

Figure 4 shows the position of the first pole T_{pol} of the Wilson-loop expectation value on the real proper-time axis for x^1 in the center of a maximum of the field strength. For small k , the pole position of the constant-field limit $E \equiv E_{\max}$ is reproduced. For large k , the pole position converges to the result of the averaged field $E \equiv E_0$. In between, the curve is not monotonically increasing, as one might have expected, but reaches T values which are significantly larger than in both limiting cases. As a consequence, the corresponding local production rate will be smaller than in the constant-field limit $E \equiv E_0$.

This behavior is, of course, a consequence of nonlocalities and can be easily understood in the worldline picture in terms of loop clouds: Starting with the limit $k \rightarrow 0$, a loop cloud sitting at a maximum detects a constant field of strength E_{\max} . A sketch of this scenario is given in Fig. 5(a). If k is increased and the wavelength of the sine becomes shorter, the loop cloud overlaps more and more with the minima on either side of the maximum and the pole moves to larger T values. If k exceeds a certain value, in our example at about $k = 0.8m$, the two minima close by dominate the Wilson-loop expectation value, Fig. 5(b). Despite the maximum in the center of the loop cloud, the pole is at a larger T value than for the averaged field. Not until the loop cloud approaches the adjacent maxima, Fig. 5(c), do the T values become smaller again, finally converging to the value of the averaged field, Fig. 5(d).

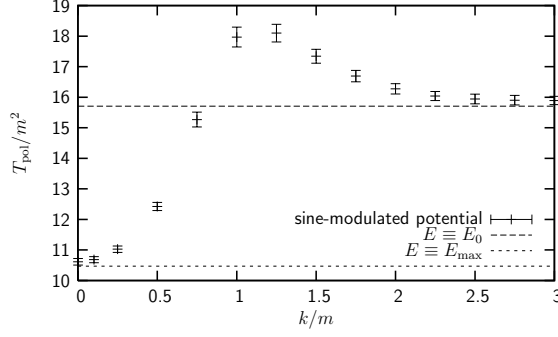


Figure 4: Position of the first pole T_{pol} of $\langle W \rangle$ on the real proper-time axis at a maximum of the field strength. With increasing frequency k , the pole moves from the constant-field limit $E \equiv E_{\text{max}}$ to the limit $E \equiv E_0$. Parameters of the field: $E_0 = 0.2(m^2/e)$, $E_{\text{max}} = 0.3(m^2/e)$. In between, it develops an unexpected maximum corresponding to a minimum of the local production rate. Parameters of the loop cloud: $n_L = 100000$, $N = 1000$ ppl.

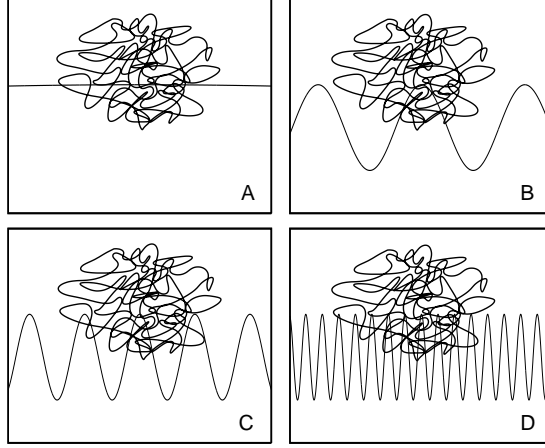


Figure 5: An artist's view on a loop cloud (worldline ensemble) at a maximum of the field strength. For small frequencies, it detects only the maximum (a). After increasing the frequency, the two nearest minima dominate (b). For larger frequencies the cloud encounters further maxima (c), until it perceives an averaged field (d).

Since the Wilson-loop expectation value at a maximum of the field strength can be dominated by the adjacent minima, the inverse situation can also occur at a minimum where the result can be dominated by the two adjacent maxima. In this case, the first pole of $\langle W \rangle$ is at a *smaller* T value than for the averaged field, leading to a *larger* imaginary part of the effective Lagrangian. This inversion is shown in Fig. 6, where the spatial distribution of the imaginary part of the effective action for $k = 1.8m$ is plotted in comparison to the constant-field limit $E \equiv E_0$. We observe that the nonlocalities induce a seemingly paradoxical phenomenon in this case: the maxima of the local pair-production rate occur at the minima of the electric field strength and vice versa.

Figure 7 depicts the imaginary part of the total effective action per space-time volume for our example configuration versus the frequency k . In contrast to its density at $x_0 = 0$, $\text{Im}\Gamma$ does not fall below the result for the averaged field. For oscillation frequencies near $k = 0$, we observe that the locally constant-field approximation based on the derivative expansion fails rather early by an order of magnitude for $k \simeq 0.5m$; this is remarkable, since the effective expansion parameter $k^2/m^2 \simeq 0.25$ might have been considered as small enough.

In the opposite limit, for large frequencies k , we obtain the averaged constant-field limit $E \equiv$

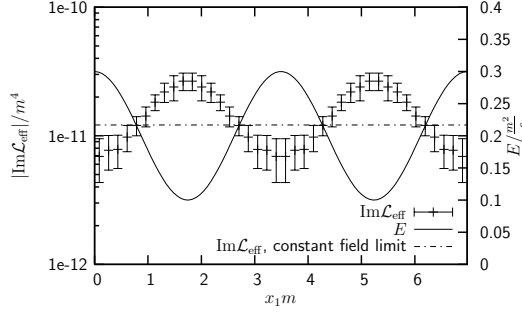


Figure 6: Spatial distribution of the imaginary part of the effective-action density for the sine-modulated potential with $k = 1.8m$ compared to the constant-field limit $E \equiv E_0$. Nonlocal effects lead to the seemingly paradoxical phenomenon that the pair-production rate is maximal at the field-strength minima and vice versa. $n_L = 200000$, $N = 1000$ ppl.

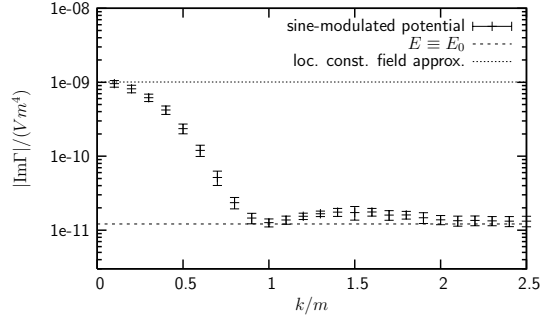


Figure 7: The imaginary part of the total effective action per space-time volume against the frequency k . The dashed lines mark the locally constant-field approximation and the result for the averaged field $E \equiv E_0$, respectively. The former (dashed lines) misses the true result by an order of magnitude already for $k/m \simeq 0.5$. $n_L = 200000$, $N = 1000$ ppl.

E_0 . It is remarkable that the imaginary part of the effective action reaches the value of the averaged field for k values as small as about $k = m$, whereas its density still fluctuates spatially for even larger k values, as seen in Fig. 6. The fluctuations cancel each other, so that they have no effect on the integrated quantity. The numerical accuracy does not eliminate the possibility of a k -dependent structure for k values larger than m . According to the values of Fig. 7, the central values suggest a slight increase of the pair production for $k > m$, until it falls back to the result for the averaged field if $k/m \rightarrow \infty$. To definitely clarify this, larger loop ensembles are necessary at the expense of CPU time. However, the present result shows that any possible k dependence for $k > m$ has to be relatively small and the averaged-field approximation yields good results in this range.

Let us finally compare our results for the spatially sine-modulated field with those for spatially homogeneous fields with time dependencies. Especially the case of an electric field oscillating in time with frequency ω has been studied with WKB methods [16, 17, 18, 19] which were originally developed for ionization processes in atomic physics [55]. The nature of pair production in this case depends on the size of the “adiabaticity parameter” $\gamma := m\omega/(eE)$; for small $\gamma \ll 1$, the result approaches the Schwinger formula and pair production thus is a nonperturbative phenomenon. For large $\gamma \gg 1$, the result becomes perturbative in $(eE)/(m\omega)$ and pair production arises from multiphoton scattering. In our case, we can, of course, also form a similar parameter⁴ $\tilde{\gamma} = mk/eE_0$, with $\tilde{\gamma}$ small or large roughly corresponding to the two limiting cases discussed above. However, it

⁴This parameter is not unique in our case, since the parameter a of the sine modulation introduces yet another scale.

is important to stress that pair production is nonperturbative in both limits for our sine-modulated field. In particular, the large- k/m (or large $\tilde{\gamma}$) case cannot be understood in terms of multiphoton processes. Taking the external field to all orders into account is essential for the final result.

6 Conclusion

We have developed a new universal approach for computing local production rates for spontaneous pair creation by the Schwinger mechanism in scalar QED. Our method is based on the combination of the worldline formalism with Monte Carlo techniques. As a first result, we have not only rediscovered Nikishov’s analytic result for the total pair-production rate in a Sauter potential, but moreover we have computed the local pair-production rate for this classic case for the first time. Most importantly, the algorithm is not restricted to any spatial symmetry of the given background potential but is applicable for arbitrary potentials.

As a nontrivial example, we have applied the algorithm to a constant electric field modulated by a spatial sine oscillation. This field configuration is representative for a whole class of fields with large-scale structures and small-scale oscillations. By varying the spatial oscillation frequency, qualitatively different features of pair production can be investigated. For small frequencies, our numerical result agrees with the derivative expansion to lowest order; the latter breaks down completely for spatial variations on the order of a few times the Compton wavelength. On this length scale and below, our results show clearly that another approximation scheme becomes reliable: the local production rate can well be approximated by inserting the *spatially averaged* field into the Schwinger formula. This averaged-field approximation can be trusted on the few-percent level for spatial variations of the size of the Compton wavelength. We would like to emphasize that the small validity bound of the derivative expansion for the imaginary part of the effective action density is not related to the same observation for the real part, as discovered in [39]; the latter arises from a subtle interplay between nonlocal quantum contributions and local counterterms, whereas the imaginary part is not affected by renormalization counterterms. Furthermore, the derivative expansion for the real part of the *integrated* effective action works well even for Compton-scale variations [56], whereas it breaks down early for the imaginary part, as displayed in Fig. 7.

Apart from these quantitative results for the particular field configurations considered here, our findings emphasize the crucial role of nonlocalities in the phenomenon of pair production. Without the feature of delocalization of a virtual pair, spontaneous vacuum decay would not occur. The worldline picture underlying our algorithm is particularly powerful in capturing these nonlocalities and, moreover, understanding their consequences in an intuitive way. Especially our results for local pair-production rates illustrate the nature and the role of nonlocalities transparently. For instance, the seemingly paradoxical situation that maxima of pair-production rates can occur at minima of the field strength (cf. Sect. 5) cannot be understood from a local approximation. However, the worldline picture identifies a natural explanation of this phenomenon in terms of the delocalization properties of the virtual pairs described by the worldline trajectory.

From a technical perspective, we have developed a numerical Monte Carlo algorithm that on the one hand requires a Euclidean formulation for the quantum fluctuations, but on the other hand produces reliable results for truly Minkowski-valued physical observables. The inherent overlap problem is solved in the present context by a physically motivated ansatz for a suitable cumulative distribution function (CDF) to which the numerical data can be fitted and that can be analytically continued to Minkowski space. Even though the success of this procedure depends strongly on the problem at hand, we believe that such techniques can be useful in other Minkowski-valued problems as well. The algorithmic strategy itself has been invented in the context of Euclidean field theory [51], where it has turned out to be highly powerful in a study of nonperturbative worldline dynamics.

Several extensions of our work are desirable and possible. So far, we have only considered spatial inhomogeneities, but any realistic field configuration will also exhibit variations in time. In fact, timelike variations bring in a new complication, since our Monte Carlo worldlines live in

imaginary time, whereas physical fields depend on real time. Therefore, our algorithm is directly applicable to all those cases where the physical field is known analytically, such that its analytic continuation to imaginary time can be evaluated and plugged into the numerics. For instance, the exact result for a solitonic profile in time direction as solved in [57] will be a benchmark test for such an investigation.

Furthermore, our results can, in principle, straightforwardly be generalized to ordinary spinor QED. As a new complication, the Pauli term $\sim \sigma_{\mu\nu} F_{\mu\nu}$ occurs in the worldline integrand. Since this term depends also on the worldline trajectory, the probability distribution function (PDF) of the ensemble will not only depend on the quantity I as defined in Eq. (17), but also on the worldline averaged Pauli-term exponential; let us denote the latter with J , which is also a scalar. Our algorithm might be generalized as follows: first, compute the PDF of J from the ensemble and bin the loops according to their J value. Then, apply the present algorithm to each J bin separately; in particular, the same analytic-continuation technique can be used. Finally, integrate over J with the aid of the PDF of J . It is important to note that the J integral can be done last, since the Pauli-term worldline average cannot induce any poles for the proper-time integral. Of course, since each relevant J bin has to contain sufficiently many worldlines, this generalization of our algorithm will at least be an order of magnitude more time consuming than the one for scalar QED. At this point, we should stress that the computations for the present work have still been performed on ordinary desktop PC's.

Finally, it is instructive to compare our method to the instanton technique of [27, 30], where the instanton approximation of the worldline integral has been shown to give the leading-order contribution to pair production. For instance, in the constant-field case, the one-pair-production rate is generated by one instanton which is a circular loop. Small fluctuations around this path lead to the correct imaginary prefactor. In comparison to this, our worldlines are extraordinarily complex. Not a single worldline loop in our ensembles resembles a circle or fluctuations thereof. This gives rise to the conjecture that the computation of the imaginary part requires very little information about the shape of the loops. We expect that we should be able to extract the instantonic content of our loops by a suitable cooling procedure that removes large-amplitude fluctuations. In view of the success of the instanton approximation, only instantonic plus small-amplitude-fluctuation information appears to be relevant for pair production. This agrees with our observation that pair production is induced by delocalized “large” loops that can acquire enough energy in the E field. Therefore, it is well possible that a different loop discretization which optimizes instantonic properties allows for an even more efficient computation of the imaginary part. A further investigation of this topic may lead to an even deeper understanding of pair production.

Acknowledgment

We are grateful to G.V. Dunne, J. Hämmerling, K. Langfeld, J. Sanchez-Guillen, M.G. Schmidt, C. Schubert, I.-O. Stamatescu, and R. Vazquez for many useful discussions, and to G.V. Dunne for helpful comments on the manuscript. This work was supported by the Deutsche Forschungsgemeinschaft (DFG) under contract Gi 328/1-3 (Emmy-Noether program).

A Constant field: straightforward approach

In the following, we present a straightforward realization of worldline numerics for calculating the pair-production rate in the constant-field case. The algorithm presented here is an immediate generalization of the standard algorithm successfully used for the real part of the effective action [37, 38, 39, 40, 41]. For a constant field in four dimensions, Eq. (5) reads

$$\Gamma_{\text{E}}^1 = -\frac{1}{(4\pi)^2} \int_0^\infty \frac{dT}{T^3} e^{-m^2 T} \int d^4 x_0 \left(\langle e^{-TeI} \rangle - 1 - \frac{1}{6} T^2 e^2 E^2 \right), \quad (21)$$

where I is defined as in Eq. (13), and the counterterms for on-shell renormalization are included. Rotating the T integration contour onto the imaginary axis and substituting $s = -iTeE$ yields a Fourier integral,

$$\Gamma_{\text{E}}^1 = \left(\frac{eE}{4\pi}\right)^2 \int_0^\infty \frac{ds}{s^3} e^{-i\frac{m^2}{eE}s} \int d^4x_0 \left(\langle e^{-iIs} \rangle - 1 + \frac{1}{6}s^2 \right). \quad (22)$$

If the worldline-ensemble average $\langle e^{-iIs} \rangle$ can be computed reliably, Eq. (22) offers a highly efficient algorithm with the aid of the FFT: in this case, Γ_{E}^1 can be computed for a whole spectrum of frequencies m^2/eE all at once with FFT. The resulting imaginary part is shown in Fig. 8. It

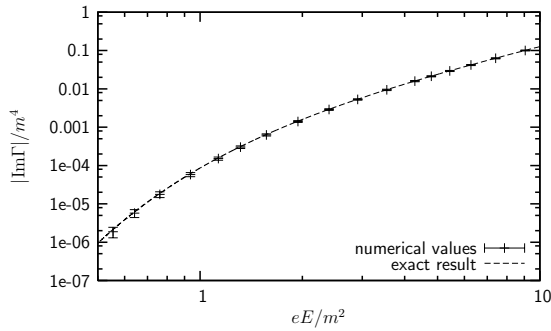


Figure 8: Imaginary part of the effective action obtained by FFT. $n_L = 5000$, $N = 1000$ ppl.

is highly remarkable that this numerical procedure gives satisfactory results in a wide range of scales, extending over five orders of magnitude, with little consumption of CPU time. However, the algorithm fails for small field strengths. The precise limit is given by the size of the largest loops in the finite loop ensemble: only loops with $|I|$ values larger than m^2/eE contribute to the imaginary part of Γ_{E}^1 . For weak fields, this implies that only a few or even no loops contribute and the computation fails.

Beside this problem which is already relevant for the constant-field case, there is a second limitation. For a different contour in the complex T plane which supports large $\text{Re}T$ values, the Wilson-loop expectation value is dominated by the loop with the largest I value. The Monte Carlo algorithms break down here, since the error bars become as large as the central value. In general, for inhomogeneous background fields, it is not possible to find a suitable integration contour to avoid this problem.

These limitations of the straightforward approach are a manifestation of the fact that the Euclidean worldline ensemble has insufficient overlap with Minkowski-valued observables for weak fields.

References

- [1] F. Sauter, Z. Phys. **69**, 742 (1931).
- [2] W. Heisenberg and H. Euler, Z. Phys. **98**, 714 (1936).
- [3] V. Weisskopf, Kong. Dans. Vid. Selsk., Mat.-fys. Medd. **XIV**, 6 (1936).
- [4] J. S. Schwinger, Phys. Rev. **82**, 664 (1951).
- [5] S. W. Hawking, Nature **248**, 30 (1974).
- [6] T. Damour and R. Ruffini, Phys. Rev. Lett. **35**, 463 (1975).
- [7] S. P. Kim and D. N. Page, arXiv:gr-qc/0401057.
- [8] A. Casher, H. Neuberger and S. Nussinov, Phys. Rev. D **20**, 179 (1979).
- [9] L. Parker, Phys. Rev. **183**, 1057 (1969).
- [10] B. Garbrecht and T. Prokopec, Phys. Rev. D **70**, 083529 (2004) [arXiv:gr-qc/0406114].

- [11] J. Arthur *et al.* [LCLS Design Study Group Collaboration], SLAC-R-0521 (1998).
- [12] G. Materlik, (ed.), T. Tschentscher, (ed.), DESY-01-011, DESY-2001-011, DESY-01-011E, DESY-2001-011E, DESY-TESLA-2001-23, DESY-TESLA-FEL-2001-05, ECFA-2001-209 (2001).
- [13] (ed.) Brinkmann, R. et al., DESY-02-167 (2002).
- [14] A. Ringwald, arXiv:hep-ph/0304139.
- [15] B. S. DeWitt, Phys. Rept. **19**, 295 (1975).
- [16] E. Brezin and C. Itzykson, Phys. Rev. D **2**, 1191 (1970).
- [17] V. S. Popov, Sov. Phys. JETP **34**, 709 (1972).
- [18] V. S. Popov and M. S. Marinov, Yad. Fiz. **16**, 809 (1972).
- [19] A. D. Piazza, Phys. Rev. D **70**, 053013 (2004).
- [20] J. Hallin and P. Liljeborg, Phys. Rev. D **52**, 1150 (1995) [arXiv:hep-th/9412188].
- [21] H. M. Fried and R. P. Woodard, Phys. Lett. B **524**, 233 (2002) [arXiv:hep-th/0110180].
- [22] J. Avan, H. M. Fried and Y. Gabellini, Phys. Rev. D **67**, 016003 (2003) [arXiv:hep-th/0208053].
- [23] S. A. Smolyansky, G. Ropke, S. M. Schmidt, D. Blaschke, V. D. Toneev and A. V. Prozorkevich, arXiv:hep-ph/9712377.
- [24] S. A. Smolyansky, A. V. Prozorkevich, S. M. Schmidt, D. Blaschke, G. Ropke and V. D. Toneev, Int. J. Mod. Phys. E **7**, 515 (1998) [arXiv:nucl-th/9709057].
- [25] Y. Kluger, E. Mottola and J. M. Eisenberg, Phys. Rev. D **58**, 125015 (1998) [arXiv:hep-ph/9803372].
- [26] R. Alkofer, M. B. Hecht, C. D. Roberts, S. M. Schmidt and D. V. Vinnik, Phys. Rev. Lett. **87**, 193902 (2001) [arXiv:nucl-th/0108046].
- [27] I. K. Affleck, O. Alvarez and N. S. Manton, Nucl. Phys. B **197**, 509 (1982).
- [28] S. P. Kim and D. N. Page, Phys. Rev. D **65**, 105002 (2002) [arXiv:hep-th/0005078].
- [29] S. P. Kim and D. N. Page, arXiv:hep-th/0301132.
- [30] G. V. Dunne and C. Schubert, arXiv:hep-th/0507174.
- [31] G. V. Dunne and T. M. Hall, Phys. Rev. D **60**, 065002 (1999) [arXiv:hep-th/9902064].
- [32] G. V. Dunne and C. Schubert, JHEP **0206**, 042 (2002) [arXiv:hep-th/0205005].
- [33] D. D. Dietrich, Phys. Rev. D **68**, 105005 (2003) [arXiv:hep-th/0302229].
- [34] D. D. Dietrich, Phys. Rev. D **70**, 105009 (2004) [arXiv:hep-th/0402026].
- [35] H. Gies, Phys. Rev. D **61**, 085021 (2000) [arXiv:hep-ph/9909500].
- [36] W. Dittrich and H. Gies, Springer Tracts Mod. Phys. **166**, 1 (2000).
- [37] H. Gies and K. Langfeld, Nucl. Phys. B **613**, 353 (2001) [arXiv:hep-ph/0102185].
- [38] H. Gies and K. Langfeld, Int. J. Mod. Phys. A **17**, 966 (2002) [arXiv:hep-ph/0112198].
- [39] K. Langfeld, L. Moyaerts and H. Gies, Nucl. Phys. B **646**, 158 (2002) [arXiv:hep-th/0205304].
- [40] H. Gies, K. Langfeld and L. Moyaerts, JHEP **0306**, 018 (2003) [arXiv:hep-th/0303264].
- [41] L. Moyaerts, K. Langfeld and H. Gies, arXiv:hep-th/0311168.
- [42] R. P. Feynman, Phys. Rev. **80**, 440 (1950).
- [43] M. B. Halpern, A. Jevicki and P. Senjanovic, Phys. Rev. D **16**, 2476 (1977).
- [44] A.M. Polyakov, “Gauge fields and strings,” Harwood, Chur, (1987).
- [45] Z. Bern and D. A. Kosower, Nucl. Phys. B **379**, 451 (1992).
- [46] M. J. Strassler, Nucl. Phys. B **385**, 145 (1992) [arXiv:hep-ph/9205205].
- [47] M. G. Schmidt and C. Schubert, Phys. Lett. B **318**, 438 (1993) [arXiv:hep-th/9309055].
- [48] M. G. Schmidt and C. Schubert, Phys. Rev. D **53**, 2150 (1996) [arXiv:hep-th/9410100].
- [49] M. Reuter, M. G. Schmidt and C. Schubert, Annals Phys. **259**, 313 (1997) [arXiv:hep-th/9610191].
- [50] C. Schubert, Phys. Rept. **355**, 73 (2001) [arXiv:hep-th/0101036].
- [51] H. Gies, J. Sanchez-Guillen and R. A. Vazquez, arXiv:hep-th/0505275, to appear in JHEP.

- [52] M. G. Schmidt and I. O. Stamatescu, Nucl. Phys. Proc. Suppl. **119**, 1030 (2003) [arXiv:hep-lat/0209120].
- [53] M. G. Schmidt and I. Stamatescu, Mod. Phys. Lett. A **18**, 1499 (2003).
- [54] A. I. Nikishov, Nucl. Phys. B **21**, 346 (1970).
- [55] L. V. . Keldysh, Sov. Phys. JETP, **20**, 1307 (1965).
- [56] N. Graham, V. Khemani, M. Quandt, O. Schroeder and H. Weigel, Nucl. Phys. B **707**, 233 (2005) [arXiv:hep-th/0410171].
- [57] G. V. Dunne and T. Hall, Phys. Rev. D **58**, 105022 (1998) [arXiv:hep-th/9807031].